Available online at www.sciencedirect.com
SCIENCE DIRECT®
Journal of Power Sources 142 (2005) 361–369
JOURNAL OF POWER SOURCES
www.elsevier.com/locate/jpowsour

Thermal batteries modeling, self-discharge and self-heating☆

Serge Schoeffert

ASB – Aerospatiale Batteries, Allée Sainte Hélène, 18021 Bourges, France

Received 11 May 2004; accepted 20 September 2004
Available online 18 December 2004

Abstract

First principal calculations made with the "Ether" code appeared pessimistic when compared with results for batteries with a duration from 50 s upwards. Subsequent examination into the reason for this confirmed that "Ether" predictions were correct in themselves, however a significant self-heating effect was necessarily taking place, this being reinforced by treatment of all the available information. The challenge for improved thermal battery modeling was then to determinate pertinent laws for this effect and to obtain accurate measurements of the phenomenon itself. An experimental method was used where the results obtained from reusable clamp stacks were subjected to mathematical treatment using "Ether". This has been successfully carried out in two similar cases and has clearly confirmed the premises: in these cases, the addition of a constant 400 W (kg of cells)$^{-1}$ internal heat generation allows for a close matching between numerical and experimental results globally, up to the exhaustion of the electrochemically active products. Correlative on the electrochemical side, when compared to single-cell tests, extended self-discharge clearly takes place in clamp stacks. Thermal batteries modeling – which has already been very useful for years – progresses toward best and appears on the way to make accurate predictions through deep physical knowledge, although there is still significant work to do.

Keywords: Thermal batteries; Modeling; Self-discharge

1. Introduction

This paper follows on from work previously presented at this conference [1]. At this stage, the "Ether" code – which associates a complex thermal model, an electrical network model and a semi-empirical electrochemical model – for thermal battery electro-thermal modeling was fully constituted and already used by battery designers, including a simplified electrochemical model. In parallel, an elaborated semi-empirical electrochemical model based on single-cell tests had been developed and used with certain success and included in a "full version" for further validation and development.

Although severely limited by other tasks, the work was pursued by confronting the a priori calculations made with this full version (with correlative entropic cooling and Joule heating but with no internal heating added, even in relation to the modeled electrical self-discharge, although it was possible), with the actual results of batteries. In direct comparison, "Ether" results were on the whole consistent for the shorter active lives. However for batteries having an active life, say, from 50 s upwards, it showed pessimistic predictions.

2. Illustration

Fig. 1 shows actual results, for a given battery design, tested at −40 °C, with the results of electro-thermal and constant-temperature calculations at different temperature values (the adiabatic temperature was calculated at 504 °C but the rule of thumb is to consider that the actual value is 20 °C higher a priori).

The case is the worst tested, because the single-cell tests (closely matched by the electrochemical model) show that

☆ Extended version of the paper presented at the 41st Power Sources Conference, Philadelphia, June 14–17, 2004.

E-mail address: s.schoeffert@asb-group.com.

0378-7753/$ – see front matter © 2004 Elsevier B.V. All rights reserved.
doi:10.1016/j.jpowsour.2004.09.038

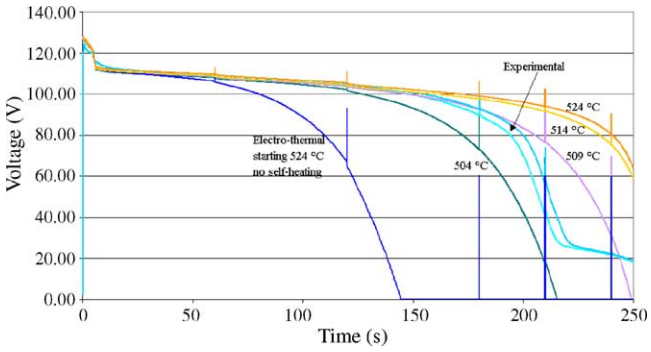

Fig. 1. Experimental and calculated voltage plots with no self-heating added, in the example case at cold temperature (−40 °C). Light blue line: experimental (×2). Deep blue line: electro-thermal simulation (starting at a stack temperature of 524 °C), with no self-heating added. Others: constant-temperature simulation (green: 504 °C; purple: 509 °C; yellow: 514 °C; orange: 524 °C).

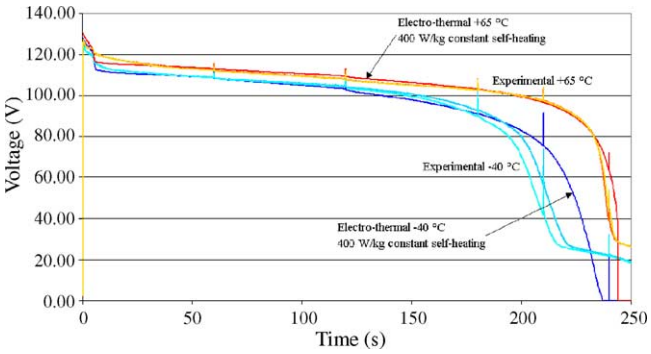

Fig. 2. Experimental and calculated voltage plots with a 400 W kg^{-1} constant self-heating added, in the example case at cold (−40 °C) and hot (+65 °C) temperatures. Light blue line: experimental at cold temperature (×2). Deep blue line: electro-thermal simulation at cold temperature with a 400 W kg^{-1} constant self-heating added. Orange line: experimental at hot temperature (×2). Red line: electro-thermal simulation at hot temperature with a 400 W kg^{-1} constant self-heating added.

the cell – an old design which includes the "precipitating" LiCl–KCl – cannot withstand the imposed current density of 0.5 A cm^{-2} for 180 s at the reference temperature value in cold condition of 500 °C. As the precipitation is a threshold mechanism, a few °C up or down greatly modify the result. However, firstly, at the cost of special precautions during manufacturing, the battery is actually reliably produced: a good simulation must reflect this fact. Secondly, for the other temperature conditions and for other batteries not in this situation, the a priori calculation results are, although resulting in a significantly better matching, also pessimistic.

3. First analysis

First of all, although the "Ether" thermal model had been closely controlled, a simple thermal calculation spreadsheet based on stationary equations and average temperatures and solved with Excel® 97 Solver was built for comparison. This had the advantage of identifying the main aspects of the problem. The match was very consistent (within 10 °C for the stack) showing once more that the thermal model was not in question. After 75 s of discharge the temperature was predicted by both modes at about 472 °C and single-cell tests show that effectively at this temperature a fresh cell cannot stand such a current longer than 50 s.

As the end heats of the battery are well designed and overcompensate slightly for the axial heat losses, the two most important phenomena involved are: (1) The entropic cooling and (2) The lateral heat losses. The impact of these is clearly shown in Appendices A and B.

However, as some input data (thermal conductivity values) were questionable, a parametric study was made, with additional comparison on the basis of skin temperature. Although some data (thermal conductivity of insulating materials) had to be significantly corrected, no combination could explain the facts with a priori calculations. The sole possible solution was that a significant internal heat generation was taking place.

The phenomenon of self-heating and its significance in thermal batteries is clearly asserted in literature [2–9] but it was not expected to have such an influence on the battery active life here. However, taken specifically, the major work of F.C. Krieger of A.N.L. in this field shows that, even after a long duration (2000 s in one case), the net sum of heat may be positive in the stack, that is to say that globally, self-heating (and Joule heating) has overcompensated the entropic cooling and lateral losses. For another battery, similar in several aspects to our example case, the value for the specific heat generation rate deduced from his data reaches a much higher level than given below (but it is not clear whether the end heats may contributed or not). In any case, this work shows clearly the possibility of a considerable impact of self-heating on performance.

All the possible self-discharge mechanisms (in a general sense) were reviewed and evaluated quantitatively for self-heating. Although some other reactions may occur and be responsible for pyrite destruction, for example, and with the exception of the eventual Li(Al)–SiO_2 reaction, only thermal or electrochemical (shorted) reactions between the electrodes active products were found to be of a nature to give significant heating. Appendix C shows clearly the order of magnitude in our example case: a few hundred (up to, around, 600) W kg^{-1} for self-heating. Fig. 2 shows the result of the electro-thermal simulation with a 400 W kg^{-1} constant internal heat production added. An interesting point is that this applies over the whole temperature domain.

Another difficulty is that as entropic cooling is an important phenomenon, the value taken for de/dT has a significant impact on the simulation result. But it is determined on adaptation on voltage plots without any regard for this. This may introduce significant errors, as stated in [4], and should be reconsidered in the future. A similar difficulty appears with the

fact that the self-heating could be related – at least in part, and possibly with some delay – to the self-discharge considered from an electrochemical point of view. While very satisfactory for prediction of the available coulombic capacity of single-cell tests, the law used to take into account the electrical self-discharge, introducing only the temperature, is far too short to reach such a self-heating (six times the value gives the same result as above).

Further proof of high self-heating was obtained by some temperature measurements that could be made easily in a special large exploratory prototype, which showed a stable temperature during its 100 s discharge and then heat-up for a very long time after current interruption. Otherwise the nature of the cathode had a large impact on the thermal balance of a battery.

4. Clamp stacks testing

So as to make a specific experimental determination of self-heating, reusable batteries – called "clamp stacks" – allowing for multiple accurate temperature measurements were designed, built and used for testing. Temperature was measured at several locations at the edge of the stack (end heat buffers, end cells, center cell), at the outer case (skin temperature) and at several positions within the lateral thermal insulation. All the measurements proved reproducible except the ones done in the lateral insulation (where very high temperature gradients require very precise positioning of the thermocouples to ensure repeatable results) and the solidification temperature plateau of electrolytes when the stack cools down appeared exactly at the expected temperature values. Fig. 3 shows the results for a 15 cells stack including a cell differing from the example cell only by thickness.

The most significant (most representative of the whole stack) result is at the center cell location. There the temperature decreases during the load and increases for a long time after the load ceased (zero external current). The reason for this behavior during the specified load is of course thought to be the effect of entropic cooling and possibly a competition between "normal" discharge and self-discharge. The maximum temperature corresponds with the fall in voltage, which it is supposed, is due to the exhaustion of the active products (the cell is far from exhaustion at the end of the specified load). Whatever the reason, self-heating (internal heat generation in the cells stack due to parasitic exothermic chemical reactions) is here again fully proven: it could be while temperature is decreasing because of lateral heat losses, it is obviously as temperature increases.

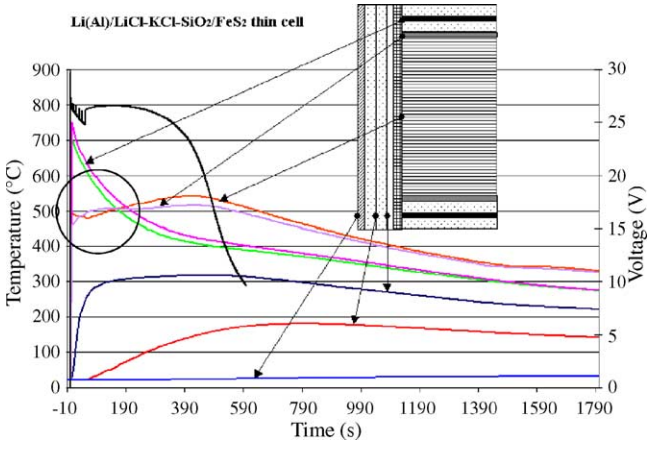

Fig. 3. Experimental results (voltage + temperatures) in a clamp stack including 15 Li(Al)/LiCl–KCl/FeS_2 thin cells tested at room temperature. Drawing: vertical half-section of the (cylindrical) battery with black dots at the thermocouples locations. Black line: voltage (right scale). Other lines: temperature plots (left scale).

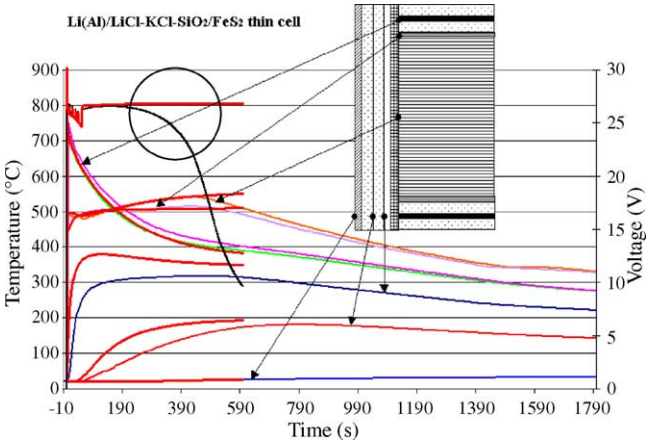

Fig. 4. Same as Fig. 3 but with corresponding electro-thermal results calculated with a 400 W kg^{-1} self-heating added. Thick red lines: simulation results.

Fig. 4 shows the superposed (in thick red lines) simulation results obtained with a constant 400 W kg^{-1} internal heat generation added (and no other modification to standards).

The match for the voltage during the load (and after for a while) and for the temperatures in the stack – especially the temperature evolution at the center cell location – and at the outer case is very good (the difficulty concerning the lateral insulation has been pointed out above). Of course, after the exhaustion of the active products, the 400 W kg^{-1} self-heating is no longer valid. This shows that a constant self-heating, until active product depletion, independent of external current is not far from reality in this case. From that, it could be concluded that the competition between external discharge and self-discharge is not strong. However the possibility of compensating mechanisms is not excluded. The other major observation is that the voltage plot falls sooner in the clamp stack than predicted from simulation, which is consistent with single-cell test results. This implies that an added self-discharge occurs in the battery, and explains the lack of correlation pointed out above between self-heating and self-discharge as deduced from single-cell tests. Figs. 5–8 show the results in the example case at ambient and cold temperatures. The results are qualitatively identical to the preceding (400 W kg^{-1} constant self-heating added as above).

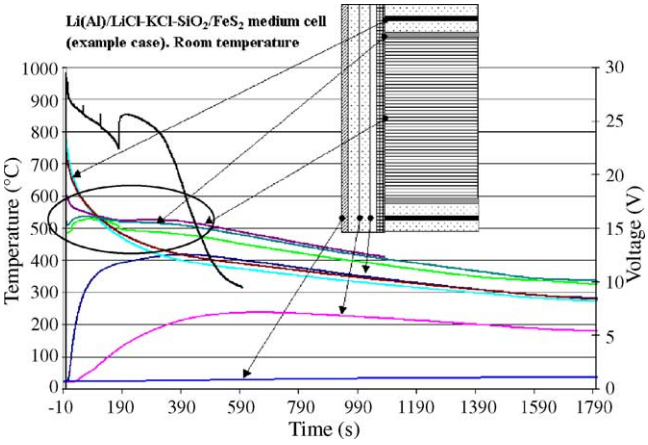

Fig. 5. Experimental results (voltage + temperatures) in a clamp stack including 15 Li(Al)/LiCl–KCl/FeS_2 medium cells ("example case") tested at room temperature.

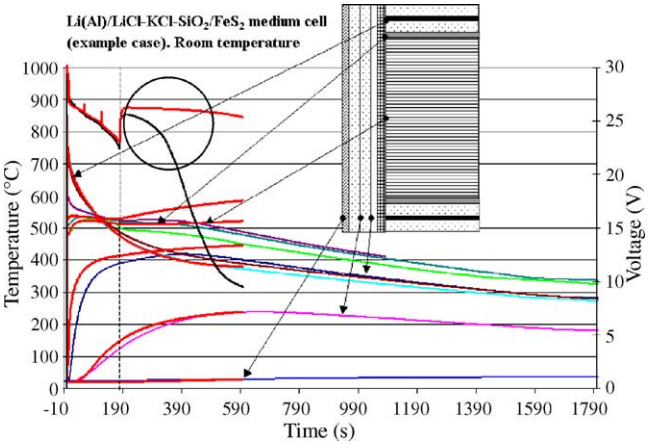

Fig. 6. Same as Fig. 5 but with corresponding electro-thermal results calculated with a 400 W kg^{-1} self-heating added. Thick red lines: simulation results.

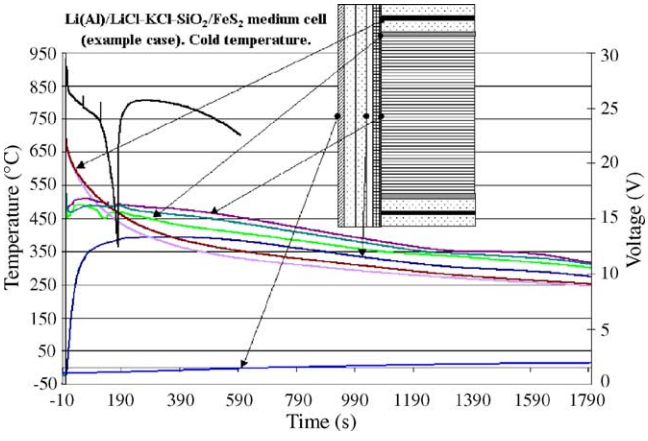

Fig. 7. Experimental results (voltage + temperatures) in a clamp stack including 15 Li(Al)/LiCl–KCl/FeS_2 medium cells ("example case") tested at cold temperature.

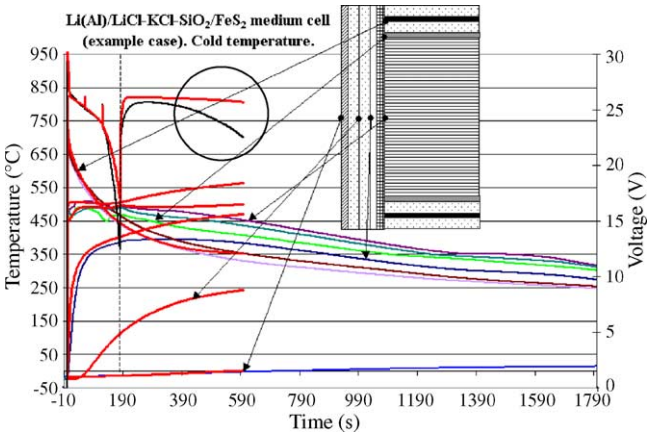

Fig. 8. Same as Fig. 7 but with corresponding electro-thermal results calculated with a 400 W kg^{-1} self-heating added. Thick red lines: simulation results.

The capability of the code to model the voltage fall at the cold initial temperature conditioning is remarkable – this fall is due to electrolyte precipitation, the difference between the actual battery and the clamp stack appearing to be the result of a simple size factor, the cell having a smaller diameter and so a lower thermal inertia in the clamp stack. However the temperature increase after load ceased is slight and short here, this being considered the consequence of the much deeper discharge during the specified load, leaving very little active material.

At this point, it appears that numerical simulation not only reveals the presence of self-heating but also closely predicts its effects.

This supposes significant further work, however:

- Supplementary expensive experimentation (clamp stacks testing) is required for the determination of self-heating for any cell in any design, with any load, etc.
- Accurate thermal conductivity values should be measured separately for this.
- As a complication, some part of the self-discharge could be due to the battery design outside the stack (and so, for example, could be specific of the clamp stack design here).
- As simple as possible laws must be defined to take it into account accurately in "Ether" in any case.

Beyond this, full control of the phenomenon requires an understanding of the physical mechanisms. Concerning the said "battery specific" self-discharge mechanisms (in addition to single-cell tests done with the standard pressure) mentioned just above, several are possible: for example, differences in pressure (axial or lateral) and so in deformation, lateral confinement, interference from the pyrotechnic chain, inter-cell currents, etc. The said "cell specific" mechanisms are briefly reviewed in the next chapter.

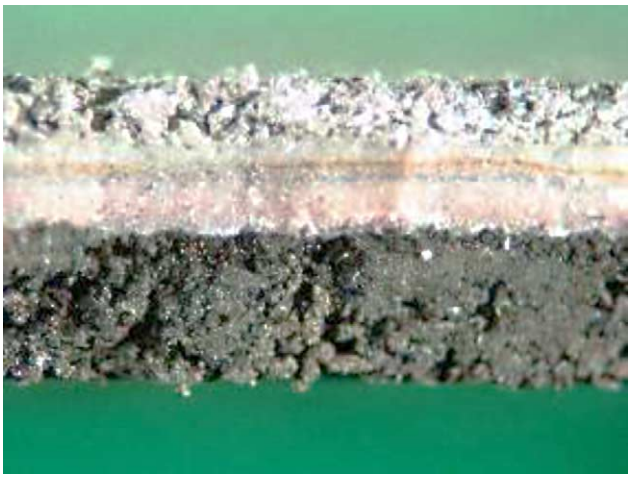

Fig. 9. Illustration of different layers that may appear in the separator layer after heating and eventual discharge. Bottom: FeS_2 positive electrode. Top: Li(Al) negative electrode.

5. Physical analysis of self-discharge

Considerable valuable work has also been carried out in the field of electrochemical self-discharge and specifically concerning the presence of "alien" compounds in the separator layer, more or less in contact with the electrodes [10–15]. Some trends about the density and width of "black" or "orange" layers (these bands are now systematically examined at ASB as part of the Research activity; Fig. 9 illustrates the phenomenon): for example, dependence on time, electrolyte nature, activity of lithium in the anode, the temperature and the current have been pointed out. However, the phenomena are so complex that no definitive mechanism has been identified.

The main trends are that, with a purified pyrite and LiCl–KCl, the sole "alien" product clearly found in the separator layer in any quantity (up to 20 vol.%), is simply lithium sulfide, Li_2S. With LiF–LiCl–LiBr, the presence of iron is attested, tending to prove that some Fe soluble specie is also involved. The main qualitative explanation given is that soluble lithium meets soluble polysulfides (and iron) in the separator. The best correlation confirms this: the volume of Li_2S – and at a lesser extent the position of the deposition front – is closely related to the activity of lithium in the anode. The intervention of gaseous sulfur in some localized overheating problems during battery development is attested otherwise in several Sandia National Laboratories papers (R.A. Guidotti & coll.).

Without going into detail, among many others (and ignoring here the intervention of O and OH species, especially in the cathode, which are known to have a significant impact through sulfide production), the following reactions (equilibria) were retained as the most probable for giving or impairing subsequent direct exothermic chemical reactions:

$FeS_2 \rightarrow 1/7\,Fe_7S_8 + 3/7\,S_2$ pyrite decomposition

$FeS_2 \rightarrow Fe^{2+} + {S_2}^{2-}$ pyrite dissolution 1

${S_2}^{2-} \rightarrow S^{2-} + 0.5S_2$ persulfide decomposition

${S_2}^{2-} + S_2 \rightarrow 2{S_2}^{-} \rightarrow {S_4}^{2-}$

per/supersulfide equilibrium

$Fe^{2+} + S^{2-} \rightarrow FeS$ iron sulfide precipitation

$FeS_2 + 6/7\,S^{2-} \rightarrow 1/7\,Fe_7S_8 + 6/7\,{S_2}^{2-}$

pyrite dissolution 2

$2Li^{+} + S^{2-} \rightarrow Li_2S$ lithium sulfide precipitation

$Li_{(l\,or\,s)} \rightarrow Li_{(g)}$ lithium vaporization

$Li_{(l\,or\,s)} \rightarrow Li_{(sol)}$ lithium dissolution

Possibly:

$FeS_2 + {S_2}^{2-} \rightarrow {FeS_2}^{-} + {S_2}^{-}$ pyrite dissolution 3

${FeS_2}^{-} + K^{+} \rightarrow KFeS_2$ $KFeS_2$ precipitation

$Li + K^{+} \rightarrow Li^{+} + K_{(g)}$ potassium inversion

The equilibrium sulfur vapor pressure for FeS_2 is 0.1 mbar at 500 °C and 10 mbar at 590 °C (it is very high for liquid sulfur as the ebullition point at 1 atm is only 445 °C; however, because of gas phase evolution, it is still present at 609 °C under 1 atm. S_2 pressure and could also exist here). The equilibrium Li (+Li_2) vapor pressure for elemental lithium is significantly lower: 5×10^{-3} mbar at 500 °C and 5×10^{-2} mbar at 590 °C. The vapor pressure of potassium is much higher (1.33 mbar at 345 °C) but the inversion itself is not favorable thermodynamically, although it has been reported experimentally by very skilled authors. The solubility value of FeS is very low: 3.2×10^{-4} (optical technique, consistent with most former values) to 4.5×10^{-7} mol% depending on S^{2-} concentration up to saturation, in LiCl–KCl at 500 °C. This excludes the coexistence of Fe^{2+} and S^{2-} or the formation of ${FeS_2}^{2-}$ to a large extent. The solubility of pyrite is not considered as known because it must be established with reference to most of the reactions listed above. However, it is probably very low, and the same for the first product of reaction of FeS_2, $Li_3Fe_2S_4$, and finally for all the reaction products of pyrite, including Fe_7S_8 (at the exception of dissociation giving soluble Li_2S and a known stable compound: e.g. Li_2FeS_2 can be seen as FeS–Li_2S). The solubility of pure lithium in LiCl–KCl is rather low, of the order of 0.01–0.5 mol% depending on authors and temperature. It should be significantly lower for alloys. Otherwise, migration tends to drive cations toward the positive (and anions toward the negative, but both with simultaneous global electrical and mechanical

equilibria). This would act as a slowing mechanism under load for the displacement of Fe^{2+} ions toward the anode.

Some other clues have been obtained at ASB from the calculation of the different yields corresponding to the three first steps (the calculation was not possible for the fourth) of discharge of FeS_2 in LiF–LiCl–LiBr at low baseline currents and high temperatures (single-cell tests).

The discharge of FeS_2 comprises four steps depending on the depth of discharge (qualitative reactions):

- $FeS_2 \rightarrow Li_3Fe_2S_4$, emf plateau (≈2.1 V/Li), 1.5 F per mole FeS_2;
- $Li_3Fe_2S_4 \rightarrow Li_{2+x}Fe_{1-x}S_2 + Fe_{1-y}S$ ($x \approx 0.2$; $y \approx 0.125$), emf plateau ≈ −0.08 V, ≈ 0.24 F per mole FeS_2;
- $Li_{2.2}Fe_{0.8}S_2 + Fe_{0.875}S$ (Fe_7S_8) → Li_2FeS_2, globally linearly decreasing emf, ≈ 0.26 F per mole FeS_2;
- $Li_2FeS_2 \rightarrow Fe + Li_2S$, emf plateau ≈ −0.50 V, 2.0 F per mole FeS_2.

The results have been partly unexpected: the yields for the two first steps were generally similar (on the preceding basis), but even when as low as 45%, the yield for the third phase was about 100%. The first conclusion was that major loss – either due to sulfur gas evolution or dissolution – left pyrrhotite, Fe_7S_8, one of the co-reactants at start of the third phase. We can note here that $Li_{2.2}Fe_{0.8}S_2$ is close to $1.1Li_2S + 0.114Fe_7S_8$, by the formula and thermodynamically. More generally, an approximate reduction of the reaction scheme to simple species is:

- $FeS_2 \rightarrow Li_3Fe_2S_4$, emf plateau (≈2.1 V/Li), 1.5 F per mole FeS_2;
- $Li_3Fe_2S_4 \rightarrow Fe_7S_8 + Li_2S$ emf plateau ≈ −0.08 V, ≈ 0.21 F per mole FeS_2;
- $Fe_7S_8 \rightarrow FeS + Li_2S$, globally linearly decreasing emf, ≈ 0.29 F per mole FeS_2;
- $FeS_{1+x} \rightarrow FeS_{1+x-dx} + dx\,Li_2S$ instantaneously, starting $FeS_{1.14}$ (Fe_7S_8), ending FeS; $0.14 \geq x \geq 0$;
- $FeS \rightarrow Fe + Li_2S$, emf plateau ≈ −0.50 V, 2.0 F per mole FeS_2.

The secondary conclusion was that in this case, a close to 100% yield for the third step means that almost no iron left the cathode.

Concerning self-discharge mechanisms, the partial (and revisable) conclusions are therefore, globally:

(1) The main product of self-discharge is lithium sulfide (although chemical analysis has not been able in some cases – with LiF–LiCl–LiBr for example – to identify it clearly). A main mechanism for self-discharge is sulfur gas, sulfur ions (polysulfides) or sulfur rich species leaving the cathode (but a simple diffusion-migration of sulfide ions may occur simultaneously). Then and more generally, all indications tend to show that the most important phenomenon is the decomposition-dissolution of pyrite. One point to examine is the reason for the non-detection of other than sulfide ions species in solution.

(2) Self-heating implies reactions between the (originally) electrochemically active materials. Despite the rather low solubility of lithium, reaction in solution of solvated elemental lithium with the soluble sulfur appears very probable, at least as a part. The other possibility is active sulfur species reaching the anode. Both gas convection and diffusion-migration in solution should be taken into account for transfer (the relative importance of both being related to the cell construction and to the temperature). Quick self-heating is most probably driven by sulfur gas convection. Dissolution is greatly enhanced by the presence of large anions (Br^-, I^- e.g.) in the electrolyte and otherwise by the wetting of pyrite particles by the electrolyte. Polysulfide ions can give sulfide ions not only by reaction with dissolved lithium but also by decomposition (liquid–gas equilibrium for sulfur tends to be reached at any location along the separator layer thickness).

(3) If extensive, elemental iron precipitation in the separator layer is of a nature to give subsequent electronic conductivity of it and subsequent "soft" short-circuits (remark: it would be also the case with dissolved elemental lithium if it did not react). But Fe^{2+} cannot exist in significant quantity in presence of sulfide ions, which have precisely been said to be in significant concentration globally. However, although not excluded a priori because of local overpotentials under load and/or presence of oxide species, and unless introduced initially by construction, the presence of significant S^{2-} ions concentration is not obvious at the vicinity of the cathode at the beginning of discharge (and a fortiori in the absence of any (external) load). The question is so left open. Another possible mechanism for iron dissolution is the displacement of a Fe–S–? anion. The precipitation of this specie in presence of K^+ would explain the absence of iron in the separator layer with a pure pyrite in LiCl–KCl. One identified candidate for this is FeS_2^-, along with the precipitation of $KFeS_2$ in LiCl–KCl. Moreover, elements given above tend to show that iron does not leave the cathode to any great extent, although this phenomenon is clearly attested qualitatively (with some attempts for quantification). A very noticeable coloration (visually) may be the result of a low proportion of the pigment. All these points require further investigation.

(4) Several other mechanisms may actually complicate the interpretation:
   - Intervention of species involving the O and OH coming from moisture pollution or built in voluntarily.
   - Intervention of halogenide ions solvating.
   - Strong unexpected capillary effects, possibly moving particles, especially in the presence of strong wetting agents (sulfide, oxide, hydroxide ions, etc.), which may be progressively produced by the reactions.
   - Dilatation or contraction of the electrodes matrix, possibly creating hydrodynamic movements of electrolyte and depending on the sulfur lost.
   - Etc.

6. Practical dispositions

The preceding analysis will be pursued and we trust in achieving it on term. However, today, it is far from giving an a priori law for self-heating. Then, the first accessible objective is simply to measure it. Making reliable (more or less micro-) calorimetric measurements on cells or batteries while discharging at up to 650 °C – which is the correct way to do it – is relatively clear in principle and such measurements at lower temperatures have actually been carried out for different battery technologies. However, on risk and economic considerations and although much more a posteriori than a priori at first, a less academic but more global way was chosen, at the imitation of F.C. Krieger past work: pursue extensive temperature measurements in clamp stacks and adapt "Ether" to deduce the heat generation rate profiles (and other values). As paradoxically, on partial bases, pure lithium (LAN) batteries seem to give much less self-heating than the considered alloy batteries, it is projected also to make extensive temperature measurements in the ASB Group high-power big batteries used in particular for torpedoes and other underwater vehicles propulsion.

7. Conclusions – perspectives

The powerful confrontation of "Ether" calculations with actual results and subsequent consolidation has brought to light the reality of very significant self-heating (necessarily tied to some kind of self-discharge, in a general sense) for some thermal battery designs. Physical knowledge about it is limited however and the first objective is now to measure it in diverse configurations. In the absence of suitable existing equipment, the method chosen is a "technical" one: the association of results obtained in instrumented reusable batteries with "Ether" calculations, which proved very efficient actually in two similar cases.

The purpose for the mathematical simulation – already considered a very good tool for battery design – to reach the level of a true and consolidated predictive tool while detailing the main phenomena occurring in thermal batteries appears reasonable although the work to be done to reach this goal is considerable. Otherwise, although not well understood physically yet, the phenomenon of self-heating is nevertheless reproducible and well controlled in a sense through final product reliability.

Acknowledgments

Acknowledgments to Janique Vigot, responsible for practical achievements and to John Reid, battery designer, for having reviewed the English formulation, both of ASB Group.

Appendix A. Entropic cooling

Entropic cooling is the name given here to the reversible heat transfer accompanying the electrochemical reactions, as it is absorbed from the immediate surroundings. That is to say concretely: the battery cools down due to its electrochemical activity. This is generally quantified through the evolution of the emf with temperature:

$$q_{\mathrm{rev}}\left(\frac{J}{C}\right) = \left[-T\left(\frac{\partial e}{\partial T}\right)\right], \qquad q_{\mathrm{rev}}(W) = \left[-T\left(\frac{\partial e}{\partial T}\right)\right] I$$

Values taken or deduced from literature (first plateaus) are:

$$\mathrm{Li/FeS_2}: q_{\mathrm{rev}} = -0.25T\ \mathrm{mJ\,C^{-1}},$$

$$\mathrm{Li/FeS_2\ at\ 800\ K}: q_{\mathrm{rev}} = -0.20\ \mathrm{J\,C^{-1}}$$

$$\mathrm{Li_{13}Si_4–Li_7Si_3/FeS_2}: q_{\mathrm{rev}} = -0.42T\ \mathrm{mJ\,C^{-1}},$$

$$\mathrm{Li_{13}Si_4–Li_7Si_3/FeS_2\ at\ 800\ K}: q_{\mathrm{rev}} = -0.34\ \mathrm{J\,C^{-1}}$$

$$\mathrm{Li(Al)_{\alpha+\beta}/FeS_2}: q_{\mathrm{rev}} = -0.48T\ \mathrm{mJ\,C^{-1}},$$

$$\mathrm{Li(Al)_{\alpha+\beta}/FeS_2\ at\ 800\ K}: q_{\mathrm{rev}} = -0.38\ \mathrm{J\,C^{-1}}$$

It is remarkable that with FeS_2 the thermoneutral potential for the first plateau is the same as for the second. For example, it is only 1.43 V for $\mathrm{Li(Al)_{\alpha+\beta}/FeS_2}$ (to be compared to 1.81 V emf at 800 K), the same as $\mathrm{Li(Al)_{\alpha+\beta}/Li_2FeS_2}$ ($q_{\mathrm{rev}} = +0.12\ \mathrm{J\,C^{-1}}$; 1.315 V emf at 800 K; close to Li(Al)/FeS(–Li_2S)), although Li_2FeS_2 is a product of discharge of FeS_2. Another way to say it is that the enthalpy of reaction per mole of electrons is about the same in both cases: $-138\ \mathrm{kJ\,F^{-1}}$ in the example.

Let us suppose a full Li(Al)/FeS_2 cell (corresponding to the example case) weighting $0.70\ \mathrm{g\,cm^{-2}}$ and having a specific heat of $0.91\ \mathrm{J\,g^{-1}\,K^{-1}}$, and so a calorific capacity of $0.64\ \mathrm{J\,cm^{-2}\,K^{-1}}$, and effectively delivering $91\ \mathrm{C\,cm^{-2}}$. Entropic cooling will absorb $91(-0.38) = -34.6\ \mathrm{J\,cm^{-2}}$, lowering the temperature by $-34.6/0.64 = -54$ °C. This is very significant for a thermal battery when just compared to its normal active temperature of (460)480–600 °C and the impact on the adiabatic temperature (about 70 °C per 100 °C; [−40; +60] °C e.g.) of the ambient temperature range.

The actual entropic cooling and Joule heating both depend on the current, and the latter on the polarization. Let us suppose the polarization can be represented by a pseudo-resistance of $0.155\ \Omega\,\mathrm{cm^2}$ and the current is $0.51\ \mathrm{A\,cm^{-2}}$ (over 178.4 s). The Joule heating is then $+40.3\ \mathrm{mW\,cm^{-2}}$ or here $+57.6\ \mathrm{W\,kg^{-1}}$, +11.2 °C and +6.3 °C/100 s while the entropic cooling is $-193.8\ \mathrm{mW\,cm^{-2}}$ or here $-276.9\ \mathrm{W\,kg^{-1}}$ and −30.3 °C/100 s. The balance is $-153.5\ \mathrm{mW\,cm^{-2}}$ or here $-219.3\ \mathrm{W\,kg^{-1}}$ and −24.0 °C/100 s. The stack would loose −42.8 °C during its discharge even in adiabatic condition, and more at a lighter current. It can be seen that the Joule heating could hardly compensate the entropic cooling, unless under exceptional current and/or internal resistance.

Appendix B. Evaluation of lateral heat losses

Let us suppose that the end heats of the battery compensate exactly the axial heat transfers. The stationary evaluation of the lateral heat transfer reported to a unit length ($W\,m^{-1}$) is given by:

$$q = -2\pi k \frac{T_i - T_e}{\mathrm{Ln}(r_e/r_i)},$$

$$\left(\mathrm{Ln}\left(1 + \frac{\Delta r}{r_i}\right) \rightarrow \frac{\Delta r}{r_i} \text{ when } \frac{\Delta r}{r_i} \rightarrow 0\right)$$

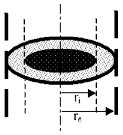

where T is the average temperature over time, r the radius and the subscripts i and e refer to the internal and external surfaces of the lateral thermal insulator, respectively, k the thermal conductivity of the latter. The stack is considered infinitely thermally conductive along a radius.

In our reference case, $k = 0.12\,W\,m^{-1}\,K^{-1}$, $r_i = 25.5\,mm$, $r_e = 32.7\,mm$, $T_i = 470\,^{\circ}C$ and $T_e = 80\,^{\circ}C$. The linear heat loss is then $-1182\,W\,m^{-1}$, representing $-211\,kJ\,m^{-1}$ over 178.4 s. With a density of $2.98\,g\,cm^{-3}$ the linear calorific capacity of the stack (which includes its full mass/diameter) is $5506\,J\,K^{-1}\,m^{-1}$. The heat loss deduced is $-38.3\,^{\circ}C$.

The insulating material has a low density of $0.07\,g\,cm^{-3}$ and a specific heat of $1.04\,J\,g^{-1}\,K^{-1}$. Its linear calorific capacity is $95.8\,J\,K^{-1}\,m^{-1}$. Its heat-up from the initial temperature of $-40\,^{\circ}C$ to the medium final temperature of $310\,^{\circ}C$ costs $33.5\,kJ\,m^{-1}$ and $-6.1\,^{\circ}C$ (for a low insulator density and a medium diameter here).

Appendix C. Thermodynamic calculations

Taken or deduced as a compromise from literature data [15,16] (enthalpy of reaction):

Formation of Li_2S at 800 K (including an analogy with Li_2O and Na_2S/Na_2O; basis: $-449.4\,kJ\,mol^{-1}$ at 298 K):

$$2Li_{(l)} + S_{(l)} \rightarrow Li_2S_{(s)} \quad -465.8\,kJ$$

$$2S_{(l)} \rightarrow S_{2(g)} \quad +108.8\,kJ$$

Dissolution of Li_2S (diluted solutions; averaged):

$$Li_2S_{(s)} \rightarrow Li_2S_{(sol,LiCl–KCl\ eut.)} \quad +50.0\,kJ$$

Remark: the sum of the four enthalpies of reaction corresponding to the four identified steps of FeS_2 discharge – including an approximation (average) for the third (decreasing) one – gives an enthalpy of formation of Li_2S at 800 K of $-453.9\,kJ\,mol^{-1}$. It is close to the value of $-465.8\,kJ\,mol^{-1}$ above (and some dissolution heat must be included in).

Phase transitions of alloys (19.7 w/0 Li for Li_yAl ((β)):

$$4/11Li_7Si_3 + Li \rightarrow 3/11Li_{13}Si_4 \quad -26.9\,kJ$$

$$Li_yAl(\beta) + \delta Li \rightarrow Li_{y+\delta}A1\,(\beta') \quad -37.9\,kJ\,mol^{-1}Li$$

$$[1/(y_\beta - y_\alpha)]Li_{y\alpha}Al\,(\alpha) + Li \rightarrow [1/(y_\beta - y_\alpha)]Li_{y\beta}Al\,(\beta) \quad -44.1\,kJ$$

Decomposition of FeS_2 (averaged, updated data):

$$FeS_2 \rightarrow 1/7\,Fe_7S_8 + 3/7\,S_2 \quad +122.2\,kJ$$

Reaction of Li with SiO_2 in local excess:

$$SiO_2 + 4Li \rightarrow 2Li_2O_{(s)} + Si \quad -304.3\,kJ$$

$$SiO_2 + Li_2O \rightarrow Li_2SiO_{3(s)} \quad -141.3\,kJ$$

$$3SiO_2 + 4Li \rightarrow 2Li_2SiO_{3(s)} + Si \quad -586.9\,kJ$$

Deduced from the preceding:

$$2Li_{(l)} + 1/2\,S_{2(g)} \rightarrow Li_2S_{(s)} \quad -520.2\,kJ$$

$$2Li_{(1)} + 1/2\,S_{2(g)} \rightarrow Li_2S_{(so1)} \quad -470.2\,kJ$$

Heats of global thermal reactions:

$$FeS_2 + 12/7\,Li \rightarrow 1/7\,Fe_7S_8 + 6/7\,Li_2S_{(s)} \quad -323.7\,kJ$$

With full dilute dissolution of Li_2S: $-280.8\,kJ$

$$FeS_2 + 36/77Li_{13}Si_4 \rightarrow 1/7\,Fe_7S_8 + 6/7\,Li_2S + 48/77Li_7Si_3 \quad -277.6\,kJ$$

With full dilute dissolution of Li_2S: $-234.7\,kJ$

$$FeS_2 + [Li_{y+\delta}A1\,(\beta')] \rightarrow 1/7\,Fe_7S_8 + 6/7\,Li_2S + [Li_yAl(\beta)] \quad -258.7\,kJ$$

With full dilute dissolution of Li_2S: $-215.9\,kJ$

$$FeS_2 + (12/7)[1/(y_\beta - y_\alpha)]Li_{y\beta}Al \rightarrow 1/7\,Fe_7S_8 + 6/7\,Li_2S + (12/7)[1/(y_\beta - y_\alpha)]Li_{y\alpha}Al \quad -248.1\,kJ$$

With full dilute dissolution of Li_2S: $-205.2\,kJ$

$$3SiO_2 + 4[1/(y_\beta - y_\alpha)]Li_{y\beta}Al \rightarrow 2Li_2SiO_{3(s)} + Si + 4[1/(y_\beta - y_\alpha)]Li_{y\alpha}Al \quad -410.5\,kJ$$

Let us now suppose that the cathode of the preceding cell contains $1.25\,mmol\,FeS_2/cm^2$ and that only 10% of it is decomposed to pyrrhotite (corresponding to an equivalent constant self-discharge current of $0.10\,A\,cm^{-2}$ over 178.4 s), the evolved sulfur reacting entirely with the $Li(Al)_{\alpha+\beta}$ of the anode. The heat of reaction ($Li_2S_{(s)}$) would be $+31.1\,J\,cm^{-2}$, giving a temperature increase of $+48.6\,^{\circ}C$. Supposing then a constant rate during 178.4 s, this gives $+174.3\,mW\,cm^{-2}$, $+249.0\,W\,kg^{-1}$ and $+27.2\,^{\circ}C/100\,s$. For comparison, a simple short-circuit (first plateaus) gives $+25.8\,J\,cm^{-2}$ (17% less).

With reference to the standard yield of 80% (but as low as 40% can be obtained for long duration batteries) $+500\,W\,kg^{-1}$ could then be obtained.

SiO_2 is sometimes used as a binder in the separator pellet along with Li(Al), exclusively – and that is the case in the example cell. This cell contains $1.3\,mmol\,cm^{-2}$ of active lithium (β phase present) and supposing that only 10% reacts with SiO_2 gives $+13.6\,J\,cm^{-2}$, $+21.3\,^{\circ}C$, $+76.3\,mW\,cm^{-2}$, $+109.0\,W\,kg^{-1}$ and $+11.9\,^{\circ}C/100\,s$.

References

[1] S. Schoeffert, "Ether": A Semi-Lumped-Parameter Model for Thermal Batteries Electro-Thermal Modeling, ASB Group, This conference, 2002 (see also: Thermal Batteries Electro-Thermal Modeling: The Semi-Lumped-Parameter Model "Ether", Aerospace Energetic Equipment 2002, Avignon, France.).

[2] D.M. Bush, R.L. Hughes (Eds.), A Thermal Model of a Thermal Battery, SAND 79-0834, Sandia Laboratories, USA, 1979.

[3] J.Q. Searcy, J.R. Armijo (Eds.), Improvements in Li(Si)/FeS_2 Thermal Battery Technology, SAND 82-0565, Sandia National Laboratories, USA, 1982.

[4] D.M. Chen, H.F. Gibbard (Eds.), Fundamental Thermal Management Aspects of the Lithium Metal Sulfide Battery, LBL-20026, Gould Inc., USA, 1985.

[5] J.D. Briscoe, D. Glen (Eds.), Thermal Model for Design Analysis of LiAl/FeS_2 Thermal Batteries, SAFT America, Inc., USA, 1986 (this conference).

[6] F.C. Krieger (Ed.), Thermal Optimization of Li(Al)/FeS_2 Thermal Batteries, Army Research Laboratory, USA, 1994 (this conference).

[7] C. Lamb (Ed.), Effects of Chemical Transport and Entropic Cooling on Long-Life Thermal Battery Designs, Including Sonobuoy Applications, Eagle-Picher Industries, Inc., USA, 1994 (this conference).

[8] F.C. Krieger (Ed.), Control of Initial Transient and Working Temperatures in Li(Al)/FeS_2 Thermal Reserve Batteries, Army Research Laboratory, USA, 1996 (this conference).

[9] F.C. Krieger, M.J. Shichtman (Eds.), Single-Pellet Thermal Batteries, U.S. Army Research Laboratory, USA, 2000 (this conference).

[10] B.J. Burow, K.W. Nebesny, N.R. Armstrong, R.K. Quinn, D.E. Zurawski (Eds.), Characterization of the Materials Comprising the Reactive Interfaces in the Li(Si)/FeS_2 Primary Battery, Sandia National Laboratories, University of Arizona, USA, J. Electrochem. Soc. 128 (9) (1981) 1919–1926.

[11] S.K. Preto, Z. Tomczuk, S. von Winbush, M.F. Roche (Eds.), Reactions of FeS_2, CoS_2 and NiS_2 Electrodes in Molten LiCl–KCl Electrolytes, Argonne National Laboratory, USA, J. Electrochem. Soc. 130 (2) (1983) 264–273.

[12] L. Redey, J.A. Smaga, J.E. Battles, R. Guidotti (Eds.), Investigation of Primary Li–Si/FeS_2 Cells, ANL-87-6, Argonne National Laboratory, Sandia National Laboratories, USA, 1987.

[13] R.A. Guidotti, F.W. Reinhardt, J.A. Smaga (Eds.), Self-discharge Study of Li-alloy/FeS_2 Thermal Cells, Sandia National Laboratories, Argonne National Laboratory, USA, 1990 (this conference).

[14] M.C. Hash, J.A. Smaga, R.A. Guidotti, F.W. Reinhardt (Eds.), Material Deposition Processes in the Separator of Li Alloy/FeS_2 Thermal Cells, SAND91-2346C, Argonne National Laboratory, Sandia National Laboratories, USA, 1991.

[15] J.R. Selman, M.L. Saboungi, Electrochemistry of sulfur in halide melts, in: R.P. Tischer (Ed.), The Sulfur Electrode. Fused Salts and Solid Electrolytes, Academic Press, 1983.

[16] M.W. Chase, JANAF Thermochemical Tables, 3rd ed., ACS/AIP/NBS, USA, J. Phys. Chem. Ref. Data, 14 (1985).